Research Article | DOI:10.5281/zenodo.12526368
www.jnanosam.com

NANOSAM
Journal of NanoScience in Advanced Materials

The Effect of Cr-doped on Structural, Magnetic and Magnetocaloric Properties of $La_{0.8}Sr_{0.15}Na_{0.05}Mn_{(1-x)}Cr_xO_3$ (x=0.00, 0.15 and 0.20) Compounds

Nadia Zaidi[1,2], Salha Khadhraoui[2,3] and Ahlem Cherif[1]

The physical properties of manganite oxides $La_{0.8}Sr_{0.15}Na_{0.05}Mn_{(1-x)}Cr_xO_3$ synthesized by solid-solid method were studied in details. X-ray diffraction analyses showed a single rhombohedral phase with $R\bar{3}c$ space group. The inhomogeneous magnetic comportment coupled was used to explain the magnetic properties and the evolution of the paramagnetic-ferromagnetic transition of the materials. The maximum values of magnetic entropy change (ΔS_{Max}) decreased from 5.77 J/Kg K for $La_{0.8}Sr_{0.15}Na_{0.05}MnO_3$ to 5.12 J/Kg K for $La_{0.8}Sr_{0.15}Na_{0.05}Mn_{0.8}Cr_{0.2}O_3$, upon an applied magnetic field of μ_{0H}=5 T, indicating an excellent quality of our samples as compared to many manganite oxides. The high quality of our samples was also checked by the large relative cooling power (RCP) which provides a good performance for industrial technologies in refrigeration device.

1. Introduction

Mixed oxides $ReAMn_{1-x}T_xO_3$ of the perovskite type where Re is a rare earth, A a monovalent cation (K^+, Na^+, Li^+), divalent (Sr^{2+}, Cd^{2+}, Ba^{2+}) or trivalent (Pr^{3+}, Nd^{3+}, Dy^{3+}) and T presents the transition metals (Fe, Ru, Cr), that have recently been the subject of numerous studies. Indeed, these compounds exhibit a variety of phases and very interesting physical properties, such as magnetoresistance and magnetocaloric effect (MCE). This MCE-based technology has brightened the horizon of refrigeration as it is more energy efficient and environmentally friendly than conventional gas expansion/compression refrigeration technology [1, 2]. More precisely, the MCE can be quantified by the magnetic entropy change ($-\Delta S_M$). Its peak is generally located near the ferromagnetic-paramagnetic (FM-PM) transition temperature (Curie temperature, T_C) [3, 4]. Magnetic refrigeration, based on MCE can replace conventional refrigeration systems, which consume a lot of energy and pollute the environment. Several studies have suggested manganese oxides as potential candidates for a possible application in this field. Additional studies are therefore necessary to optimize the structural, magnetic and electrical properties of these oxides [5].

The particular properties of these perovskite-type manganese oxides result from the fact that they lie between a paramagnetic-semiconductor state and a metallic ferromagnetic state [6]. Partial substitution of the rare earth (Re) ions by a divalent, monovalent ion or a stoichiometric defect results in the oxidation of the Mn^{3+} ion to Mn^{4+}. This mixed oxidation of Mn is the basis for the various changes in the physical properties of these oxides. In particular, structural and magnetic transitions due to slight distortions of the structure are frequently encountered. In fact, there are other factors that have a significant impact on the properties of these materials such as the production method, the temperature, the duration of annealing and the size of the elements occupying the different sites (A or B) [7, 8].

In terms of the crucial role of Mn site, it would be interesting and worthwhile to study the effects of Mn-site element substitution, which may provide clues for exploring novel MCE materials and concerning the mechanism of MCE. Within this

[1]Department of Physics, College of Sciences, Jouf University, Aljouf, Saudi Arabia. [2]University of Monastir, Faculty of Science of Monastir, Laboratory of Physical Chemistry of Materials, Department of Physics, Monastir, Tunisia.[3]Physics Department, Faculty of Science, AL-Baha University, Al Bahah, Saudi Arabia.

#Corresponding author: nszaidi@ju.edu.sa

Keywords: Manganite oxides; magnetocaloric; Magnetization; Magnetic entropy change.

Received: 21 November 2023 | Accepted: 02 February 2024 | Published online: 30 June 2024

framework, the effect of substituting trivalent ions such as Fe, Ni and Sc for Mn^{3+} ions in the B site on the ferromagnetic properties of these manganites has been studied [9]. It was experimentally found that any modification on the exchange interaction causes the reduction in Curie temperature T_C. However, differently from the common ionic substitution, Cr doping in manganites has a peculiar effect and is attracting more attention. A slight substitution of Cr for Mn ions favors the formation of the ferromagnetic metal (FMM) states [10].

$La_{0.8}Sr_{0.15}Na_{0.05}O_3$ is one of the perovskite compounds which possess physical properties [11]. Potential applications, particularly magnetic refrigeration (MR) require a transition temperature T_C close to room temperature. This can be achieved by an appropriate amount of oxygen stoichiometry or by the substitution of Mn by a non-magnetic or magnetic cation. So, to decrease the critical temperature and enhance the physics properties of the parent compound $La_{0.8}Sr_{0.15}Na_{0.05}O_3$, we made a substitution of Chromium (Cr) for manganese (Mn). Then, we investigated the effect of this substitution on the physical properties of $La_{0.8}Sr_{0.15}Na_{0.05}O_3$.

2. Results and Discussion

2.1. Scanning electron microscopy and energy dispersion spectroscopy

Polycrystalline samples of $La_{0.8}Sr_{0.15}Na_{0.05}Mn_{1-x}Cr_xO_3$ series with (=0.00, 0.15 and x=0.20) were prepared by conventional solid state ceramic processing. High purity (99.99 %) starting compounds La_2O_3, Cr_2O_3, MnO_2, Na_2O and $SrCO_3$ were taken in stoichimetric proportions. Care was taken to remove moisture before weighing by preheating the precursors at 873 K for 12 h. The mixtures were heated in air at 1073 K for 24 h to achieve decarbonization. After grinding, they were heated at 1373 K for 48 h and ground again to ensure homogeneity. The intermediate steps of cooling and mechanical grinding were repeated in order to achieve accurate homogenization and complete reaction. The powders were pressed into pellets and sintered at 1673 K for 72 h under an Ar/H_2 (5%) atmosphere with several intermediate grinding and repulsions. Finally, these pellets were quenched to room temperature. The elemental composition and the homogeneity of the samples were studied by X-ray microanalysis (energy dispersion spectroscopy, EDS) coupled with a Scanning Electron Microscopy (SEM). An example of the EDS spectrum obtained for the x = 0.2 sample is shown in Figure 1. The characteristic peaks of the chemical elements (La, Sr, Na, Mn, Cr and O), were clear, which confirms the presence of all the elements introduced during the preparation.

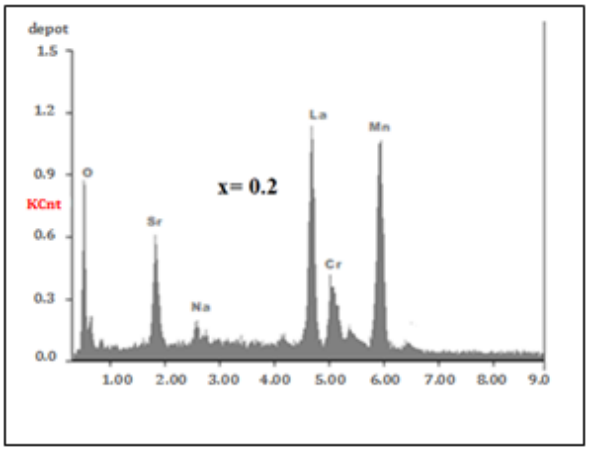

Figure 1. Spectra Obtained by Analysis by EDS and Micrograph for the Compounds $La_{0.8}Sr_{0.15}Na_{0.05}Mn_{1-x}Cr_xO_3$ Compounds (x = 0.2).

The SEM photo of $La_{0.8}Sr_{0.15}Na_{0.05}Mn_{1-x}Cr_xO_3$ (x=0.00, 0.15 and x=0.2) compounds (Figure.2) shows strongly bonded polycrystalline grains with very negligible porosity. For all samples, we can see that the grains exhibit spheroid-like shapes and a good connectivity between each other. This facilitates the intrinsic behaviors, because good current percolation between grains and the opening up of conduction channels do not block the ordering of the Mn spins. The grain size was calculated using the intercept technique. We draw a random straight line through the micrograph and count the number of grain boundaries that intersecting this line. The average grain size was calculated by dividing the number of intercepts by the actual line length. Furthermore, the grain size decreased with the addition of Cr content in LSNMCr0.2 and averaged 153.2 nm compared to 144.3 nm grain size of the LSNMCr0.00 samples. Cr substitution reduced the grain size and the density because of the chemical diffusion of covalent ions to optimize the compositional homogeneity.

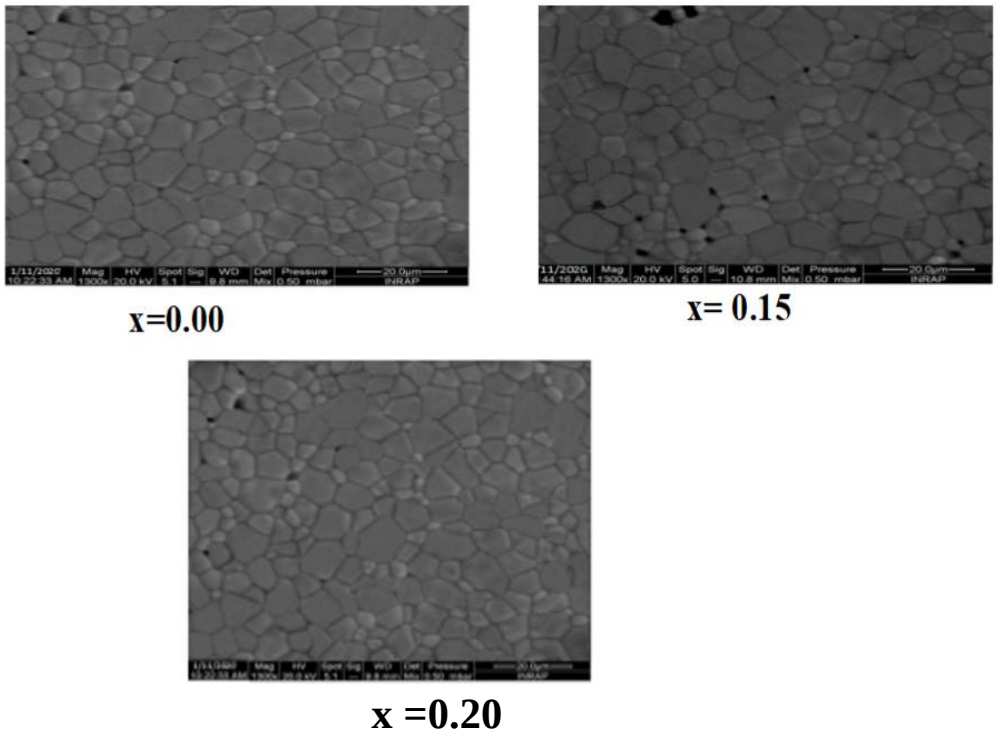

Figure 2. The SEM photo of $La_{0.8}Sr_{0.15}Na_{0.05}Mn_{1-x}Cr_xO_3$ (x=0.00, 0.15 and x=0.2) compounds.

2.2. Determination of Grain Size

We calculated the average grain size D_{sc} using the following Scherrer's formula [12-14];

$$D_{sc} = \frac{0.9\lambda}{\beta \cos\theta} \quad (1)$$

where λ is the wavelength of x-radiation, θ is Bragg angle for the most intense peak (104). $\beta = \sqrt{\beta_m^2 - \beta_s^2}$, β_s corresponds to the most intense peak of silicon serving as a standard and β_m is the width at half height of the peak (FWHM).

Table 2. The Average Grain Sizes Obtained by Scherrer's Formula and by SEM, Variation of the tolerance factor as a function of the mean radii $<r_A>$ and $<r_B>$ for different substitution rates x.

x	0	0.15	0.2
β (10^{-3}) rad	2.95	2.88	2.82
2θ (°)	32.69	32.701	32.711
D_{SC} (nm)	48.44	47.89	47.22
D_{SEM} (nm)	153.171	148.75	144.32
$< r_A >$(Å)	1.2373	1.2373	1.2373
$< r_B >$ (Å)	0.626	0.619	0.608
t	0.927	0.91	0.904
D (nm)	49	48.42	48.06
Strain (δ)	0.146	0.147	0.148

We noticed that the grain size decreased with the increase in the substitution rate x. The values of grain size observed by the SEM were higher than those observed by Scherrer's formula. This difference can be explained by the fact that each particle observed by the SEM is made up of many granules [15]. Scherrer's formula currently remains the most significant [16]**.** According to Table.1, the tolerance factor t decreased slightly when the mean radius increased, that is, when the rate of substitution of Mn^{3+} by Cr^{3+} increased. Therefore, we expected, rhombohedral or orthorhombic structural deformations for these compounds.

2.3. Structural characterization of materials by X-ray diffraction (XRD)

The X-ray diffraction measurements of the raw data on the samples prepared in the form of crystalline powder were carried out in the X-ray department of the Borj Cédria technopole using an automatic two-circle powder diffractometer «Panalytical X'Pert PRO Systems» equipped with a cobalt anticathode (λ_{cobalt} = 1.789 Å). The diffractograms were recorded in (Bragg –Brentano) mode in the angular domain: ranging from 90° ≤ 2θ ≤ 110°. The X-ray diffraction diffractograms (Figure. 3) showed rather fine and intense lines, which

NANOSAM
Journal of NanoScience in Advanced Materials

implies the good crystallization of the synthesized samples. Structural analysis was carried out by the Rietveld method [17] using the FullProf program (version 2009). This method is based on a minimization by the method of least squares of the difference between the observed and the calculated profiles of the powder diffractogram. The structure analysis was performed in the hexagonal space group R$\bar{3}$c. The refinement results are illustrated in (Table.2). The different tuning factors determining the quality of treatment and controlling the results of adjustments are; the Rwp-weighted profile residual, the statistical test χ^2 of fit that tends to (1) for successful refinement, and the residual on R_F structure factors.

Table 3. Rietveld refinement results of $La_{0.8}Sr_{0.15}Na_{0.05}Mn_{1-x}Cr_xO_3$ (x=0.00, 0.15 and x=0.2) compounds.

X	0	0.15	0.20
Space group R$\bar{3}$c			
a (Å)	5.5491	5.5342	5.5288
c (Å)	13.4533	13.4421	13.4366
V (Å^3)	359.442	358.377	357.89
R_{wp} (%)	3.40	3.11	3. 05
R_p (%)	2.61	2.42	2.18
R_F	5.44	4.19	3.45
χ^2 (%)	1.52	1.43	1.33
B (K$^{-3/2}10^{-5}$)	1.92	1.26	1.04
D (meV Å ^{2})	7.53	10.75	14.77

Table 2 shows that the values of a and c as well as the volume of the crystal lattice decreased as a function of the substitution rate x for the $La_{0.8}Sr_{0.15}Na_{0.05}Mn_{1-x}Cr_xO_3$ solid solutions. This change in volume V can be explained by the decrease in the arithmetic radius of the cations occupying the B site during the substitution of manganese (0.65 Å) by chromium with a smaller radius (0.64 (Å). Figure.3 shows the X-ray diffraction diffractograms obtained after refinement by the "Rietveld" method for $La_{0.8}Sr_{0.15}Na_{0.05}Mn_{1-x}Cr_xO_3$(x=0.00, 0.15 and 0.20) compounds. The observed difference between the measured and calculated intensity is almost negligible except at the level of the most intense peak.

Williamson-Hall approach was used to find close values, for deconvoluting size and strain contribution to the X-ray line broadening. According to this approach, the X-ray line broadening is due to the contribution from small crystallite size and the broadening caused by the lattice strain present in the material [18], i.e.

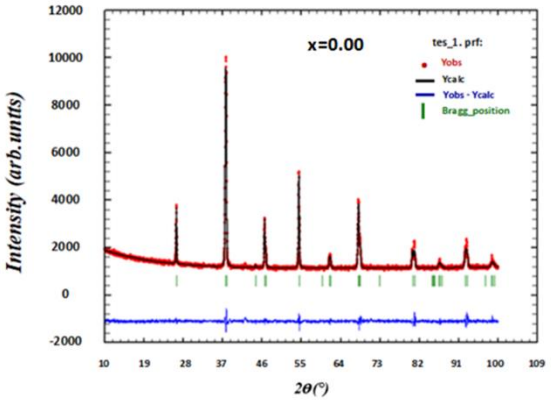

(a)

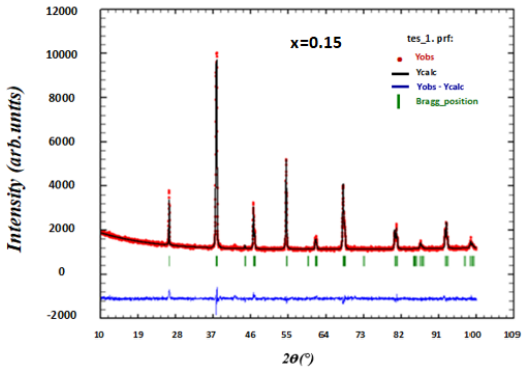

(b)

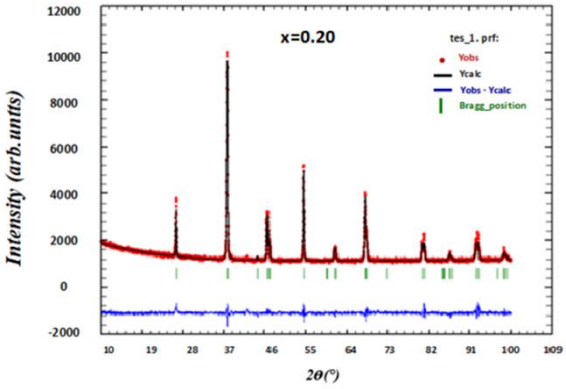

(c)

Figure 3. Refined Rietveld for $La_{0.8}Sr_{0.15}Na_{0.05}Mn_{1-x}Cr_xO_3$(x=0.00, 0.15 and 0.20) compounds.

$$\beta = \beta_{size} + \beta_{strain} \quad (2)$$

Where $\beta_{size} = \frac{k\lambda}{D\cos\theta}$ *and* $\beta_{strain} = 4\delta tang\theta$,

where δ is strain $\frac{\Delta l}{l}$, so *3* becomes

$$\beta = \frac{k\lambda}{Dcos\theta} + 4\delta tang\theta \quad (3)$$

NANOSAM
Journal of NanoScience in Advanced Materials

$$\beta \cos\theta = \frac{k\lambda}{D} + 4\delta \sin\theta \quad (4)$$

Where, 4δ is a measure of strain present in the lattice. By plotting $\beta cos\theta$ vs. $4sin\theta$, we can find the crystallite size from the intercept ($\frac{k\lambda}{D}$) of this line on the y axis and the slope of the line gives the strain (δ).

Strain measurements for all samples are plotted in Figure.4. The strain measured from the slope increased with increasing Cr doping, which indicates that strain increases as larger Cr ion accommodates in MnO_3 matrix. The plots have shown a negative strain for $La_{0.8}Sr_{0.15}Na_{0.05}Mn_{1-x}Cr_xO_3$ series with (x=0.00, 0.15 and 0.20) compounds. This may be due to the lattice contraction observed in the calculation of lattice parameters. The low value of lattice strain may be due to the fact that the synthesis procedure did not impose much constraint in the formation of compound as it is generally found in case of extensive ball milling technique, strained layer growth, etc. [15, 19]. The crystallite-size (D) and the strain (δ) for all samples are listed in Table.1. The crystallite size calculated in the present system using the Willam-Hall technique was larger than the crystallite size (D_{Sc}) because the broadening effect due to strain is completely excluded in Debye-sheerer technique [20].

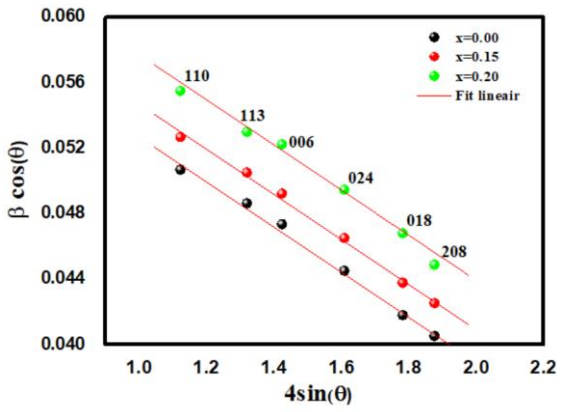

Figure 4. Variation of strain graph for $La_{0.8}Sr_{0.15}Na_{0.05}Mn_{1-x}Cr_xO_3$ for (x=0.00, 0.15 and 0.2) samples.

2.4. Magnetic study

The investigation of the magnetic properties measured in a magnetic field of 0.05 T confirmed that all samples exhibited simple FM/PM phase transitions, as shown in Figure 5. Curie temperature (T_C) was determined at inflection point of dM/dT curves of the samples. The ferro-paramagnetic transition temperatures were 355 K, 285 K and 271 K for x=0.00, 0.15 and x=0.20 respectively. It should be noted here that the magnetic transition temperature T_C decreased upon increasing the substitution rate of Cr. This decrease was very slow, indicating that the ionic substitution of Cr systematically reduces the domain of ferromagnetism. Indeed, the substitution of Mn by Cr weakned the ferromagnetic interactions Mn^{3+}- O- Mn^{4+}, Mn^{3+}- O- Cr^{3+}, and enhanced antiferromagnetic interactions Mn^{3+}- O- Mn^{3+}, Mn^{4+}- O- Mn^{4+}, Cr^{3+}- O- Cr^{3+}. With the increase in the level of Chromium, the competition between the ferromagnetic interactions and the antiferromagnetic interactions increased, which decreased magnetization [21, 22].

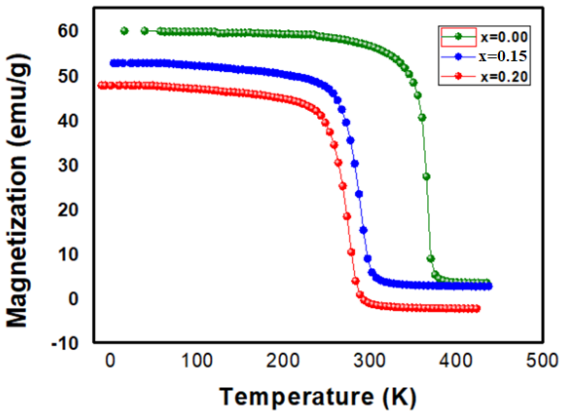

Figure 5. Magnetization vs Temperature for the Compounds $La_{0.8}Sr_{0.15}Na_{0.05}Mn_{1-x}Cr_xO_3$ (x = 0.00, 0.15 and 0.20) under the effect of a field of 0.05T.

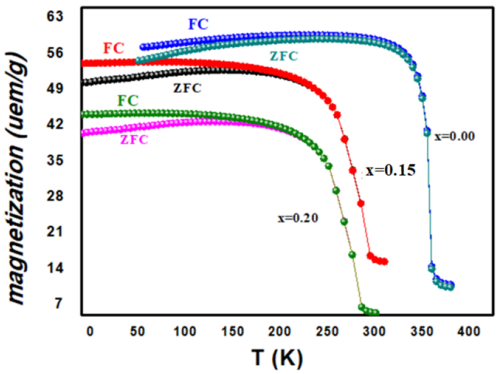

Figure 6. Temperature dependences of the zero-field-cooled and field-cooled magnetization for $La_{0.8}Sr_{0.15}Na_{0.05}Mn_{1-x}Cr_xO_3$ (x=0.00, 0.15 and x=0.2) compounds under applied magnetic field 0.05 T.

Figure 6 shows the temperature dependence of the zero field-cooled (ZFC) and field-cooled (FC) magnetization for x=0.00, 0.15 and x=0.20 samples. As can be seen, all the samples undergo a transition from a ferromagnetic to a paramagnetic phase. It is clear that the 'FC' curves do not coincide with the

'ZFC' curves below T_C. This seems very clear, especially for samples x=0.15 and x=0.20. However, the curves 'FC' and 'ZFC' curves have a common part for the high temperature, wherein the variation of magnetization with temperature is reversible and superposed. At low temperature, the behavior is irreversible with a divergence between 'ZFC' and 'FC'. The magnetic moment decreases gradually. Such irreversibility in the M-T data for the FC and 'ZFC' measurements was observed in several manganite systems and it was suggested that this irreversibility is possibly due to the canted nature of the spins or to the random freezing of spins [23].

The low temperature thermal evolution of magnetization was fitted to Bloch's $T^{3/2}$ law. According to this law, the zero-field magnetization M(T) should have temperature dependence [24]:

$$\frac{M(T,\mu_0 H)}{M(0,\mu_0 H)} = 1 - BT^{\frac{3}{2}} \quad (5)$$

Where M(0, μ_0H) was obtained by extrapolating M(T, μ_0H) curves to T=0 K using a second- order polynomial and M(T, μ_0H) is the spontaneous magnetization at finite temperature. The prefactor B is a characteristic constant of the spin waves at low temperature, which can be written as [25]:

$$B = 2.612\frac{g\mu_B}{M(0)}\left(\frac{K_B}{4\pi D}\right)^{3/2} \quad (6)$$

Where g ≈ 2 is the gyromagnetic ratio for electrons, μB is Bohr's magneton, K_B is Boltzmann constant and D is the spin wave stiffness constant. The stiffness D is defined by spin wave dispersion relation [26]:

$$E(q) = \Delta + Dq^2 \quad (7)$$

Where E(q) is the spin wave energy, q is the wave vector and D is the gap arising from the anisotropy of the applied magnetic field. In our analysis we assume Δ=0. The curve Ln (1-M(T, μ_0H)/M(0, μ_0H)) vs. Ln(T) in the inset of (Figure. 7) was used to show that our compounds obey Bloch's $T^{3/2}$ law. It has predicted that the slope of the linear fit of this curve must be close to 3/2. The slopes were formed to be equal to 1.493, 1.435 and 1.415 for x= 0.00, x=0.15 and x=0.20, respectively. Figure 7 shows the reduced magnetization M (T, μ_0H)/M(0. μ_0H) as a function of $T^{3/2}$ for μ_0H=0.05T (T ≤ 90K) for $La_{0.8}Sr_{0.15}Na_{0.05}Mn_{0.85}Cr_{0.15}O_3$. The slope of the linear fit plot of the data M(T, μ_0H)/M(0, μ_0H) vs. $T^{3/2}$ provided B values from which the values of the spin stiffness constant D were determined. The values of B and D are shown in Table. 2. This result shows that there is a spin-wave excitation in our samples. The obtained values of D are comparable to those found in the ground state of other FM insulating manganites such as $La_{0.8}Ca_{0.2}MnO_3$ [27]. Moreover, they are in an excellent agreement with those reported for other polycrystalline manganites [28].

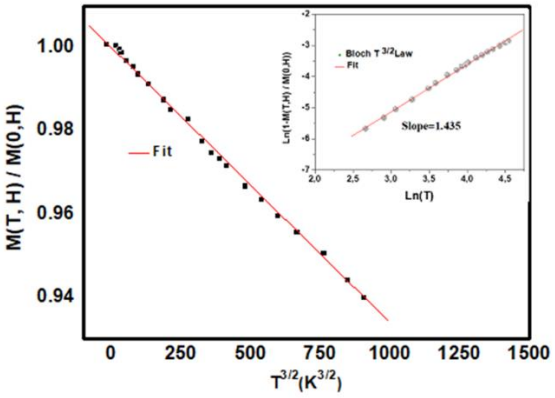

Figure 7. Plot of M (T, μ_0H) /M(0, μ_0H) vs. $T^{3/2}$ of $La_{0.8}Sr_{0.15}Na_{0.05}Mn_{0.85}Cr_{0.15}O_3$ at μ0H, The inset shows the variation of Ln(1- M(T, μ_0H)/M(0, μ_0H)) vs. Ln($T^{3/2}$) to determine the slope of the linear curve.

2.5. Magnetocaloric Effect

2.5.1. Determination of Magnetic Entropy

The magnetocaloric effect is defined by the change in adiabatic temperature and the change in isothermal entropy. Our samples were characterized by means of magnetization measurements, which allow access to the entropy variation [21]. To determine the nature of the magnetic transition of the samples. Arrott's isotherms; μ_0H/M were used as a function of M^2 around T_C (Figure 8). According to the Banergie criterion [29]. The curve μ_0H/M as a function of M^2 showed a positive slope, indicating that the ferromagnetic-paramagnetic transition is of the second order. These measurements allow to quantify the behavior of entropy as a function of temperature according to Maxwell's relation[30].

$$\Delta S_M\left(\frac{T_1+T_2}{2}\right) = \frac{1}{T_2-T_1}\left[\int_0^{\mu_0 Hmax\int} M(T_2,\mu_0 H)\mu_0 dH - \int_0^{\mu_0 Hmax\int}(M(T_1,\mu_0 H)\mu_0 dH\right] \quad (8)$$

NANOSAM
Journal of NanoScience in Advanced Materials

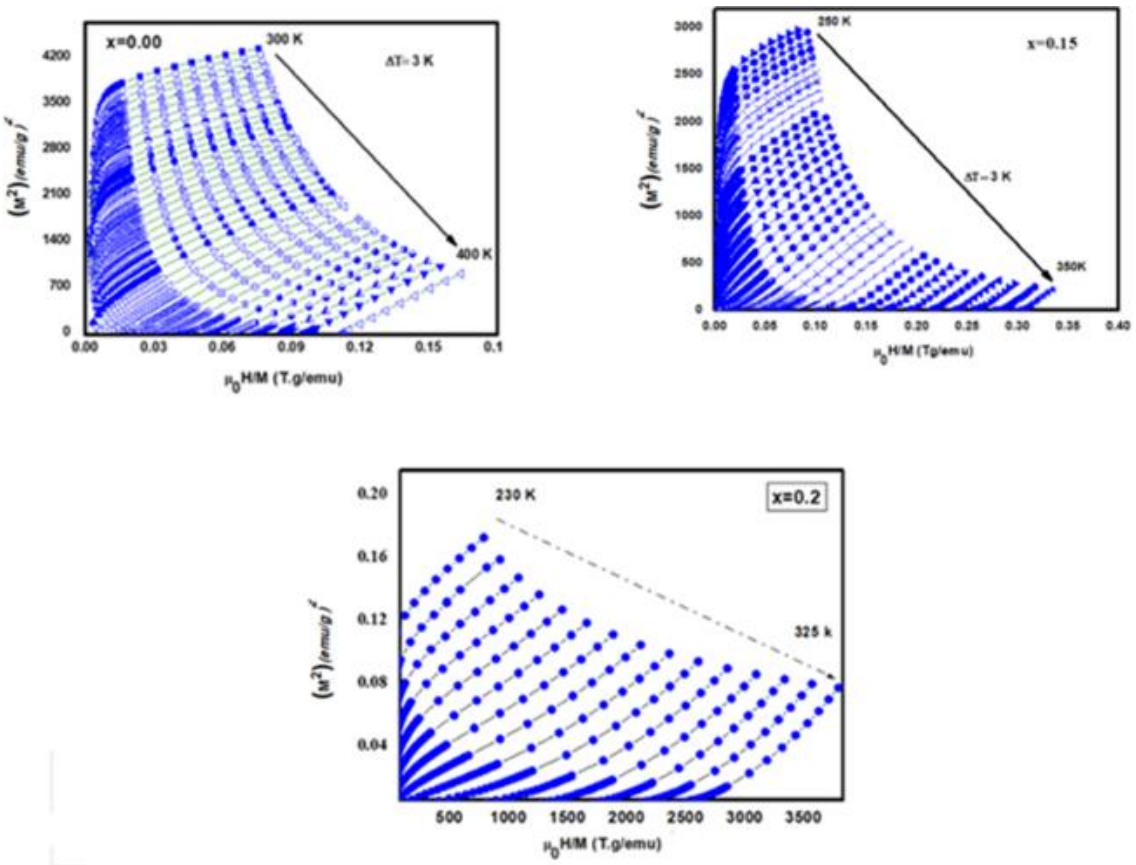

Figure 8. Variation of $\mu_0 H/M$ vs M^2 for $La_{0.8}Sr_{0.15}Na_{0.05}Mn_{1-x}Cr_xO_3$ (x = 0.00, 0.15 and 0.20) compounds.

This amounts, for each temperature, to calculating the air between two isotherms around the temperature in question over the desired field range divided by the temperature difference between these two curves. The maximum magnetic-entropy value decreased from 5.77 J/kg/K for x=0.00 to 5.12 J/kg/K for x= 0.2 near their respective T_C at 5 T. Figure.9 shows the variation of the magnetic entropy change as a function of temperature for $La_{0.8}Sr_{0.15}Na_{0.05}Mn_{1-x}Cr_xO_3$ (x = 0.00, 0.15 and 0.20) samples determined under an applied magnetic field of 5 T. These curves revealed that the maximum of the magnetic entropy change ($|\Delta S_M^{max}|$) decreased when increasing Cr-concentration. This change can be explained by the characteristic fusion of chromium atoms with the rest of the sample atoms as temperatures rise, resulting in a reduction the framework of the fluctuations of the magnetic moments interaction. In fact, Zener's model [31] is strongly recommended to explain this property of the large magnetocaloric effect in manganites. Moreover, Guo et al. [34, 35] explain the large value of ΔS_M by the stronger spin-lattice coupling detected by a simultaneous variation of structural distortion and the magnetic transitions [31-33].

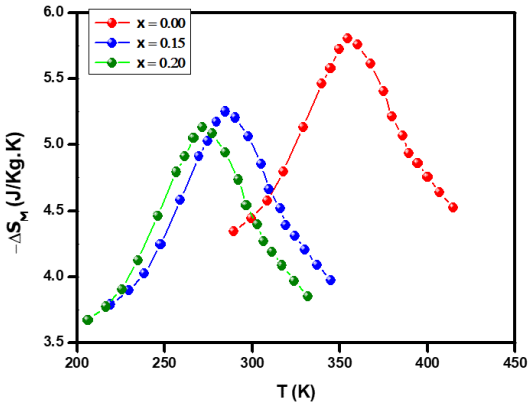

Figure 9. Variation of magnetic entropy vs temperature with different magnetic fields for the $La_{0.8}Sr_{0.15}Na_{0.05}Mn_{1-x}Cr_xO_3$ (x = 0.00, 0.15 and 0.20) compounds.

Theoretically and experimentally [34, 35] there is relationship between ΔS_M^{max} and H. Magnetic materials with second order transition obey $\Delta S_M^{max} = -kM_s(0)h^{2/3}$, where h is a reduced field[$h = (\mu_0\mu_B H)/(k_B T_C)$, k is a constant, $M_s(0)$ is the saturation magnetization at low temperatures and S(0.0) is the reference parameter, Which is opposite to zero [34]. ΔS_M^{max} as a function of $h^{2/3}$ are plotted in Figure. 10. We are analyzed these results

NANOSAM
Journal of NanoScience in Advanced Materials

Table 3. Comparison of ΔS_M^{max} and (RCP) for the compounds $La_{0.8}Sr_{0.15}Na_{0.05}Mn_{1-x}Cr_xO_3$ (x = 0.00, 0.15 and 0.20) observed at T_C under the effect of magnetic field $\mu_0 H$ = 5 T with some materials considered interesting in the application of magnetic refrigerators.

Composition	T_c (K)	$\mu_0 \Delta H$	$\lvert\Delta S_M^{max}\rvert$ (J/Kg K)	RCP (J/Kg)	References
$La_{0.6}Pr_{0.1}Sr_{0.3}MnO_3$	360	5	3.32	227.44	[35]
$La_{0.6}Pr_{0.1}Sr_{0.3}Mn_{0.95}Ru_{0.05}O_3$	350	5	3.11	214.14	[35]
$La_{0.6}Pr_{0.1}Sr_{0.3}Mn_{0.85}Ru_{0.15}O_3$	344	5	2.57	188.68	[35]
$La_{0.52}Dy_{0.15}Pb_{0.33}MnO_3$	290	5	3.51	246	[36]
$Gd_5 (Si_2Ge_2)$	275	5	18.5	535	[37]
$La_{0.8}Ba_{0.2}Mn_{0.1}Fe_{0.1}O_3$	193	5	2.62	211	[38]
$La (Fe_{0.96}Co_{0.04})_{11.9}Si_{1.1}$	243	5	22.5	-	[39]
$La (Fe_{0.94}Co_{0.06})_{11.9}Si_{1.1}$	274	5	20	-	[39]
$La_{0.8}Sr_{0.15}Na_{0.05}Mn\ O_3$	355	5	5.77	298	Our work
$La_{0.8}Sr_{0.15}Na_{0.05}Mn_{0.85}Cr_{0.15}O_3$	285	5	5.25	294	Our work
$La_{0.8}Sr_{0.15}Na_{0.05}Mn_{0.8}Cr_{0.2}O_3$	271	5	5.12	290	Our work

and found that the sign of S (0,0) is negative, which is expected for second order magnetic transition (SOMT) [34]. The linear dependence of ΔS_M^{max} versus $h^{2/3}$ implies the strong localization of moments and the second order transition in $La_{0.8}Sr_{0.15}Na_{0.05}Mn_{1-x}Cr_xO_3$ (x = 0.00, 0.15 and 0.20).

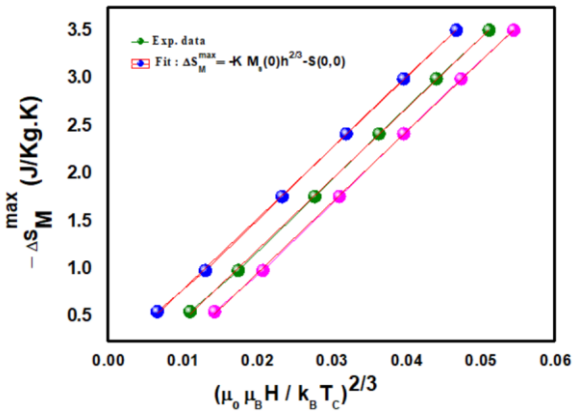

Figure 10. Temperature dependence of magnetic entropy change $-\Delta S_M^{max}$ versus $h^{2/3}$ for $La_{0.8}Sr_{0.15}Na_{0.05}Mn_{1-x}Cr_xO_3$ (x = 0.00, 0.15 and 0.20). compounds.

2.5.2. Determination of the relative cooling power (RCP)

Relative cooling power, RCP, is defined as the amount of heat transferred from the hot source to the cold source in a refrigerator [21].

$$RCP = -\Delta S_M^{max} \times \delta T_{FWHM} \quad (9)$$

For a 5 T field, the obtained RCP values were of the order of 298, 294 and 290, for x = 0.00, 0.15 and 0.20 respectively. To better assess the applicability of our $La_{0.8}Sr_{0.15}Na_{0.05}Mn_{1-x}Cr_xO_3$ compounds in the application magnetic refrigeration, the values of $\lvert\Delta S_M^{max}\rvert$ and RCP obtained for this series were compared with several materials having an acceptable T_C and considered to be promising for this application (Table 3). Our compounds exhibited an accepted entropy change, which indicates that they could be considered as potential candidates for magnetic refrigeration.

2.5.3. Dependence of Magnetic Entropy Change

The magnetic field dependence on the magnetic entropy changes ΔS_M at a temperature T for materials obeying a second-order phase transition follows an exponent power law of the type [40, 41]: $\Delta S_M = b(\mu_0 H)^n$:

$$n = \frac{d \ln \Delta S_M}{d \ln H} = -\frac{\mu_0 H}{\Delta S_M}\left(\frac{\partial M}{\partial T}\right)_H \quad (10)$$

Where b is a constant and the exponent n depends on the values of field and temperature. By fitting the data of ΔS_M versus $\mu_0 H$, we obtained the value of n as a function of temperature at different magnetic fields for example x=0.00, as depicted in Figure.11. From this figure, the exponent n was close to 1 in the FM regime and increased to 2 in the PM regime. The exponent n exhibited a moderate increase with decreasing temperature and took extreme values around Curie temperature of the existing phase, then sharply increased with increasing temperature. In a mean field approach, the value of *n* at Curie temperature is predicted to be 2/3 [40].

NANOSAM
Journal of NanoScience in Advanced Materials

For manganites the exponent was roughly field independent and approached approximate values of 1 and 2, far below and above the transition temperature respectively [41]. Then, the values of n around T_C were 0.583, 0.604 and 0.612 for x=0.00, 0.15 and 0.20 respectively, which confirms the probability of 3D Ising model and 3D Heisenberg model to describe our material. These values are similar to those obtained for soft magnetic materials containing rare earth metals [40, 41].

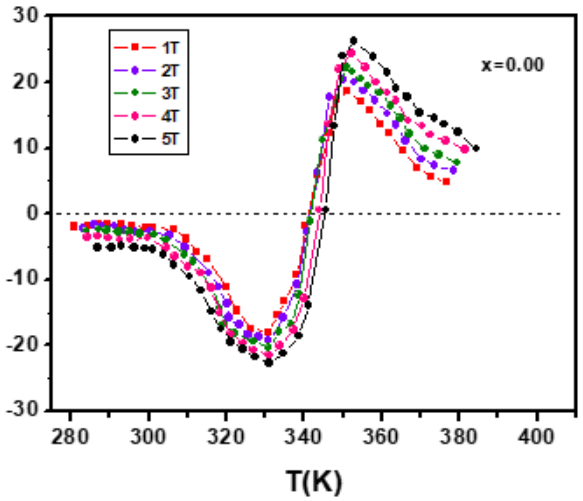

Figure 11. Change of specific heat of the sample as a function of temperature at different magnetic fields for x = 0. 00.

3. Conclusion

In this work, we synthesized solid solutions of $La_{0.8}Sr_{0.15}Na_{0.05}Mn_{1-x}Cr_xO_3$ (x = 0.00, 0.15 and 0.20). Then, we studied the influence of Cr substitution on the Structural, magnetic and magnetocaloric properties of our samples. The samples were prepared by the standard ceramic process. They showed single-phase and crystallized in a rhombohedral structure with $R\bar{3}c$ space group. T_C decreased slowly by substituting Cr for Mn. We also found that the entropy changes and the relative cooling power during the phase transition decreased with the increase in Cr. These observations indicate that the existence of Cr weakens the ferromagnetism in the $La_{0.8}Sr_{0.15}Na_{0.05}Mn_{1-x}Cr_xO_3$ perovskite. Finally, we investigated the correlation between critical exponents and magnetocaloric effect. The values of n confirm the probability of 3D Ising model and 3D Heisenberg model to describe our material.

Authors' contributions:

All authors have equal contributions to the current work.

Data Availability Statement

The data that support the findings of this study are available from the corresponding author upon reasonable request.

References

[1] Ncib, W., Ben Jazia Kharrat, A., Wederni, M.A., Chniba-Boudjada, N., Khirouni, K., and Boujelben, W. Investigation of structural, electrical and dielectric properties of sol-gel prepared La0.67-xEuxBa0.33Mn0.85Fe0.15O3 (x=0.0, 0.1) manganites, Journal of Alloys and Compounds **768** 249-262 (2018).

[2] Khedmi, N., Zaidi, N., and Hsini, M. Magnetocaloric Effect Simulation in La0.8Na0.2MnO3-Δ Nanopowders, Journal of NanoScience in Advanced Materials **2** (1) 25-30 (2023).

[3] Al-Yahmadi, I.Z., Gismelseed, A.M., Al Ma'Mari, F., Al-Rawas, A.D., Al-Harthi, S.H., Yousif, A.Y., Widatallah, H.M., Elzain, M.E., and Myint, M.T.Z. Structural, magnetic and magnetocaloric effect studies of Nd0.6Sr0.4AxMn1-xO3 (A=Co, Ni, Zn) perovskite manganites, Journal of Alloys and Compounds **875** 159977 (2021).

[4] Hsini, M., khadhraoui, S., Zaidi, N., and Alrowaili, Z.A. Modeling the Magnetocaloric Effect of La0.67Pb0.33MnO3 by the Mean-Field Theory, Journal of Superconductivity and Novel Magnetism **31** (11) 3717-3722 (2018).

[5] Lyubina, J. Magnetocaloric materials for energy efficient cooling, Journal of Physics D: Applied Physics **50** (5) 053002 (2017).

[6] Zaidi, N. and Cherif, A. Critical behavior and magnetocaloric effect simulation in TbFeSi and DyFeSi intermetallic compounds using a Landau universal, AIP Advances **13** (4) (2023).

[7] Sun, L., Zhang, R., Ni, Q., Cao, E., Hao, W., Zhang, Y., and Ju, L. Magnetic and dielectric properties of MgxCo1-xFe2O4 ferrites prepared by the sol-gel method, Physica B: Condensed Matter **545** 4-11 (2018).

[8] Ju, J., Lin, J., Wang, Y., Zhang, Y., and Xia, C. Electrical performance of nanostructured strontium-doped lanthanum manganite impregnated onto yttria-stabilized zirconia backbone, Journal of Power Sources **302** 298-307 (2016).

[9] Reshmi, C.P., Savitha Pillai, S., Suresh, K.G., and Varma, M.R. Room temperature magnetocaloric properties of Ni substituted La0.67Sr0.33MnO3, Solid State Sciences **19** 130-135 (2013).

[10] Wang, Z.H., Geng, D.Y., Gong, W.J., Li, J., Li, Y.B., and Zhang, Z.D. Effect of adding Cr on magnetic properties and metallic behavior in MnTe film, Thin Solid Films **522** 175-179 (2012).

[11] Tozri, A., Alhalafi, S., Alrowaili, Z.A., Horchani, M., Omri, A., Skini, R., Ghorai, S., Benali, A., Costa, B.F.O., and Ildiz, G.O. Investigation of the magnetocaloric effect and the critical behavior of the interacting superparamagnetic nanoparticles of La0.8Sr0.15Na0.05MnO3, Journal of Alloys and Compounds **890** 161739 (2022).

[12] Mnefgui, S., Zaidi, N., Dhahri, A., Hlil, E.K., and Dhahri, J. Behavior of the magnetocaloric effect and critical exponents in La0.67Sr0.33Mn1−xVxO3 manganite oxide, Journal of Solid State Chemistry **215** 193-200 (2014).

[13] Moghadam, R.Z., Dizagi, H.R., Agren, H., and Ehsani, M.H. Understanding the effect of Mn2+ on Yb3+/Er3+ co-doped NaYF4

upconversion and obtaining the optimal combination of these tridoping, Scientific Reports **13** (1) 17556 (2023).

[14] Zarei Moghadam, R., Ehsani, M.H., Rezagholipour Dizaji, H., Kameli, P., and Jannesari, M. Oxygen doping effect on wettability of diamond-like carbon films, Materials Research Express **8** (3) 035601 (2021).

[15] Zhang, K.S., Xue, J.N., Wang, Y.X., Sun, H., and Long, Y. Magnetocaloric effect and corrosion resistance of La(Fe, Si)13 composite plates bonded by different fraction of phenolic resin, AIP Advances **8** (4) (2017).

[16] Cong, D.Y., Huang, L., Hardy, V., Bourgault, D., Sun, X.M., Nie, Z.H., Wang, M.G., Ren, Y., Entel, P., and Wang, Y.D. Low-field-actuated giant magnetocaloric effect and excellent mechanical properties in a NiMn-based multiferroic alloy, Acta Materialia **146** 142-151 (2018).

[17] Liu, J., Li, G., and Fathy, H.K. A Computationally Efficient Approach for Optimizing Lithium-Ion Battery Charging, Journal of Dynamic Systems, Measurement, and Control **138** (2) (2015).

[18] Mohamed, Z., Tka, E., Dhahri, J., and Hlil, E.K. Giant magnetic entropy change in manganese perovskite La0.67Sr0.16Ca0.17MnO3 near room temperature, Journal of Alloys and Compounds **615** 290-297 (2014).

[19] Chen, L., Li, Y., Zhang, Q., and Hao, X. Electrical properties and energy-storage performance of (Pb0.92Ba0.05La0.02)(Zr0.68Sn0.27Ti0.05)O3 antiferroelectric thick films prepared by tape-casing method, Ceramics International **42** (11) 12537-12542 (2016).

[20] Rao, K.S., Tilak, B., Varada Rajulu, K.C., Swathi, A., and Workineh, H. A diffuse phase transition study on Ba2+ substituted (Na0.5Bi0.5)TiO3 ferroelectric ceramic, Journal of Alloys and Compounds **509** (25) 7121-7129 (2011).

[21] Zaidi, N., Mnefgui, S., Dhahri, A., Dhahri, J., and Hlil, E.K. The effect of Dy doped on structural, magnetic and magnetocaloric properties of La0.67−xDyxPb0.33MnO3 (x=0.00, 0.15 and 0.20) compounds, Physica B: Condensed Matter **450** 155-161 (2014).

[22] Belo, J.H., Amaral, J.S., Pereira, A.M., Amaral, V.S., and Araújo, J.P. On the Curie temperature dependency of the magnetocaloric effect, Applied Physics Letters **100** (24) (2012).

[23] Li, G., Li, Q., Pan, M., Hu, B., Chen, C., Teng, J., Diao, Z., Zhang, J., Jin, R., and Plummer, E.W. Atomic-Scale Fingerprint of Mn Dopant at the Surface of Sr3(Ru1−xMnx)2O7, Scientific Reports **3** (1) 2882 (2013).

[24] Giri, S.K., Dasgupta, P., Poddar, A., and Nath, T.K. Tuning of normal and inverse magnetocaloric effect in Sm0.35Pr0.15Sr0.5MnO3 phase separated manganites, Journal of Alloys and Compounds **631** 266-271 (2015).

[25] Zaidi, N., Mnefgui, S., Dhahri, A., Dhahri, J., and Hlil, E.k. Study of electrical transport and magnetoresistive properties of La0.67−x DyxPb0.33 MnO3 (x = 0.00, 0.10 and 0.15), Journal of Alloys and Compounds **616** 378-384 (2014).

[26] Gómez, A., Chavarriaga, E., Supelano, I., Parra, C.A., and Morán, O. Tuning the magnetocaloric properties of La0.7Ca0.3MnO3 manganites through Ni-doping, Physics Letters A **382** (13) 911-919 (2018).

[27] Jiang, W., Zhou, X., Williams, G., Mukovskii, Y., and Glazyrin, K. Griffiths phase and critical behavior in single-crystal La0.7Ba0.3MnO3: Phase diagram for La1-xBaxMnO3 (x<0.33), Physical Review BGriffiths phase and critical **77** (6) 064424 (2008).

[28] Jiang, W., Zhou, X., Williams, G., Mukovskii, Y., and Glazyrin, K. Is a Griffiths Phase a Prerequisite for Colossal Magnetoresistance?, Physical Review Letters **99** (17) 177203 (2007).

[29] Tlili, R., Hammouda, R., Bejar, M., and Dhahri, E. Theoretical investigation of the magnetocaloric effect on La0.7(Ba, Sr)0.3Mn0.9Ga0.1O3 compound at room temperature, Journal of Magnetism and Magnetic Materials **386** 81-84 (2015).

[30] Shen, T.D., Schwarz, R.B., Coulter, J.Y., and Thompson, J.D. Magnetocaloric effect in bulk amorphous Pd40Ni22.5Fe17.5P20 alloy, Journal of Applied Physics **91** (8) 5240-5245 (2002).

[31] Zener, C. Interaction between the d-Shells in the Transition Metals. II. Ferromagnetic Compounds of Manganese with Perovskite Structure, Physical Review **82** (3) 403-405 (1951).

[32] Ribeiro, P.O., Alho, B.P., Alvarenga, T.S.T., Nóbrega, E.P., de Sousa, V.S.R., Carvalho, A.M.G., Caldas, A., de Oliveira, N.A., and von Ranke, P.J. Theoretical investigations on magnetocaloric effect in Er1−yTbyAl2 series, Journal of Magnetism and Magnetic Materials **379** 112-116 (2015).

[33] Nath Mahato, R., Sethupathi, K., Sankaranarayanan, V., and Nirmala, R. Co-existence of giant magnetoresistance and large magnetocaloric effect near room temperature in nanocrystalline La0.7Te0.3MnO3, Journal of Magnetism and Magnetic Materials **322** (17) 2537-2540 (2010).

[34] Dong, Q.-y., Zhang, H.-w., Shen, J.-l., Sun, J.-r., and Shen, B.-g. Field dependence of the magnetic entropy change in typical materials with a second-order phase transition, Journal of Magnetism and Magnetic Materials **319** (1) 56-59 (2007).

[35] Zaidi, N., Mnefgui, S., Dhahri, J., and Hlil, E.K. Effect of Ru substitution on the physical properties of La0.6Pr0.1Sr0.3Mn1−xRuxO3 (x = 0.00, 0.05 and 0.15) perovskites, RSC Advances **5** (40) 31901-31909 (2015).

[36] Banerjee, B.K. On a generalised approach to first and second order magnetic transitions, Physics Letters **12** (1) 16-17 (1964).

[37] Pecharsky, V.K. and Gschneidner, J.K.A. Giant Magnetocaloric Effect in Gd5Si2Ge2, Physical Review Letters **78** (23) 4494-4497 (1997).

[38] Ghodhbane, S., Dhahri, A., Dhahri, N., Hlil, E.K., and Dhahri, J. Structural, magnetic and magnetocaloric properties of La0.8Ba0.2Mn1−xFexO3 compounds with 0⩽x⩽0.1, Journal of Alloys and Compounds **550** 358-364 (2013).

[39] Hu Feng-Xia , Q.X.-L., Wang Guang-Jun , Sun Ji-Rong , Shen Bao-Gen , Cheng Zhao-Hua , Gao Ju. Magnetoresistances and magnetic entropy changes associated with negative lattice expansions in NaZn₁₃-type compounds LaFeCoSi, Chin. Phys. B **14** (11) 2329-2334 (2005).

[40] Franco, V., Conde, C.F., Blázquez, J.S., Conde, A., Švec, P., Janičkovič, D., and Kiss, L.F. A constant magnetocaloric response in FeMoCuB amorphous alloys with different Fe⁄B ratios, Journal of Applied Physics **101** (9) (2007).

[41] Nisha, P., Savitha Pillai, S., Varma, M.R., and Suresh, K.G. Critical behavior and magnetocaloric effect in La0.67Ca0.33Mn1−xCrxO3 (x = 0.1, 0.25), Solid State Sciences **14** (1) 40-47 (2012).